Self-Assembly of Linactants: Micelles and Lyotropic Liquid Crystals in Two Dimensions

Stephanie M. Malone,[†] Siwar Trabelsi,[†] Shishan Zhang,[‡] T. Randall Lee,[‡] and Daniel K. Schwartz*,[†]

Department of Chemical and Biological Engineering, University of Colorado, Boulder, Colorado 80309-0424, and Department of Chemistry, University of Houston, Houston, Texas 77204-5003

Received: May 13, 2010

We report observations of phenomena within two-component Langmuir monolayers that are analogous to surfactant self-assembly in 3D solutions. A partially fluorinated fatty phosphonic acid played the role of 2D surfactant (linactant), and a perfluorinated fatty acid acted as the 2D solvent. Langmuir−Blodgett monolayers were prepared from mixtures of these compounds and examined using atomic force microscopy. Above a critical linactant mole fraction of ∼0.013, distinctive monodisperse structural features were observed with a characteristic diameter of ∼30 nm and a relative height of 1.4 nm. As the linactant concentration was further increased, the number density of these features increased linearly with concentration, whereas the size remained approximately the same. A quantitative analysis of these observations suggested that the features corresponded to self-limiting clusters composed of ∼2000 linactant molecules and that the dispersed clusters represented a 2D micellar phase. Above a linactant mole fraction of 0.63, the clusters organized into a local hexagonal structure with short-range positional order indicative of a 2D "lyotropic" liquid crystalline phase; the correlation length increased systematically with increasing linactant concentration.

Introduction

The aggregation of surfactants into micelles is the classic example of molecular self-assembly and is also technologically important for applications such as detergency, emulsification, nanoparticle synthesis, and others. Above a critical micelle concentration (CMC) in aqueous solution, monodisperse surfactant aggregates form spontaneously, giving rise to an isotropic phase in which micelles are dispersed in dilute surfactant solution.[1,2] As the surfactant concentration is increased further above the CMC, the concentration of micelles rises systematically, whereas the micelle size and monomer concentration remain approximately constant. At very high surfactant concentrations, micelles may organize into quasi-periodic structures known as lyotropic liquid crystal (LC) phases.[3]

The classical treatment of micelle thermodynamics is based on a mass action aggregation model first proposed by Debye[4] and further developed by Tanford.[5,6] This model, involving an equilibrium between N surfactant monomers and aggregates with an equilibrium constant K, provides a surprisingly accurate description of the aggregation process and gives an approximate value of the CMC $\approx (NK)^{-1/N}$. It has been suggested theoretically that the thermodynamic formation of micelles could occur in two dimensions (2D) within molecular monolayers;[7] however, 2D micellar dispersions have never been observed experimentally. In this article, we report observations of 2D phenomena that are directly analogous to micelles and lyotropic LCs in molecular monolayers composed of two components that represent surfactant and solvent, respectively. This phenomenon represents an important piece of current efforts to understand surfactancy (or to be more precise, line activity) in 2D systems such as lipid monolayers, bilayers, and biological membranes[8−15] because, as in three dimensions, 2D micelles represent a reservoir of available line-active molecules.

Langmuir monolayers (LMs) of insoluble surfactants are particularly appropriate for studies of 2D thermodynamics because the dynamic nature of the liquid−vapor interface permits a high degree of self-organization, and the thermodynamic parameters (surface pressure, temperature, molecular area) can be directly measured and controlled. LMs have been employed extensively as model systems for studies of thermodynamics/phase transitions in quasi 2D biological systems, including cell membranes,[8,16] pulmonary surfactants,[17−19] and biomimetic sensors.[20,21] Langmuir−Blodgett (LB) transfer of LMs to a solid substrate[22−24] (e.g., by dipping) permits the application of additional characterization methods such as AFM.

In previous work, we considered mixed monolayers of fluorinated and hydrogenated fatty acids that separated into hydrocarbon-rich and fluorocarbon-rich 2D phases. We found that the addition of various partially fluorinated fatty phosphonic acids significantly reduced the line tension between these 2D phases,[25,26] and we coined the term "linactant" for these line-active compounds. The concept of line activity has a long history[8] in the context of the formation of finite-sized lipid domains within monolayers, bilayers, and biological membranes (e.g., lipid rafts) and remains an area of active experimental[10−12,14,15] and theoretical[9,13] interest. However, these partially fluorinated surfactants represented the first successful example of compounds rationally designed for line activity at a particular 2D interface. We also found that in pure one-component monolayers, many of these linactants spontaneously formed modulated phases exhibiting quasi-periodic structures.[27,28] Related phases have been observed in other films composed of partially fluorinated compounds,[29−39] and the nanometer-scale structure in these phases has been ascribed to the incompatibility of the close-packing preferences of hydrocarbon and fluorocarbon substituents. The present experiments were pursued to determine

* To whom correspondence should be addressed. E-mail: Daniel.Schwartz@colorado.edu. Tel: 303-735-0240. Fax: 303-492-4341.
[†] University of Colorado.
[‡] University of Houston.

10.1021/jp104375s
Published on Web 06/16/2010

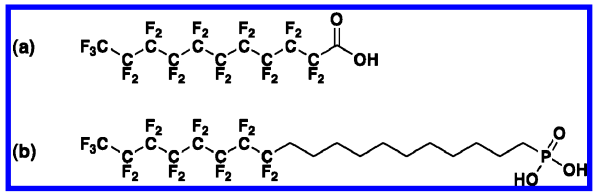

Figure 1. Structures of (a) the perfluorinated fatty acid (**F10**) and (b) the partially fluorinated linactant (**F8H11**) used in this work.

whether such compounds would exhibit properties consistent with micellization in a 2D solution.

Materials and Methods

Langmuir Monolayers and Langmuir−Blodgett Deposition. Monolayers were prepared in a Nima LB trough using 0.5 g/L solutions of perfluoroundecanoic acid (**F10**, 96% Oakwood Products) in chloroform (99.9% Fisher) and 0.1 to 1.0 g/L solutions of 12,12,13,13,14,14,15,15,16,16,17,17,18,18,19,19-heptadecafluorononadecyl phosphonic acid (**F8H11**, synthesis previously described[27]) in tetrahydrofuran (99.9% Fisher). Figure 1 shows the molecular structures of the two compounds. The subphase consisted of Millipore water (18.2 MΩ) adjusted to pH 3 with HCl (37% Mallinckrodt). After spreading, monolayers were left for 15 min to permit solvent evaporation. The monolayer was compressed to a surface pressure of 4 mN/m with a barrier speed of 20 mm/min and maintained at this pressure during LB transfer to freshly cleaved mica by vertical dipping at 10 mm/min on the upstroke. Isotherms were performed with identical spreading procedures, and allowing the solvent to evaporate for 30 min, with a barrier speed of 20 mm/min. Because of instability of the pure **F8H11** monolayer at high surface pressures, its isotherm was shifted horizontally to its predicted position based on extrapolated area/molecule data from **F8H11/F10** mixtures. Monolayers of both **F8H11** and **F10** were quite stable at moderate surface pressures, however. Isobaric stability experiments found that the surface area varied by only ∼0.5% for **F8H11** and ∼1.5% for **F10** during the entire time required for LB transfer at the relevant temperature and surface pressure. These drift rates resulted in a negligible change to the nominal mole fraction for all mixtures studied.

AFM Imaging and Image Analysis. Samples were imaged with a Nanoscope III (Digital Instruments, now Veeco) multimode AFM under ambient conditions using silicon tips with a nominal spring constant of 40 N/m and a nominal tip radius of 10 nm. Images were obtained in tapping mode using height contrast at room temperature (23 ± 1 °C). The distinctive features (representing 2D micelles) on the AFM images were counted using ImageJ for mole fractions of 0.63 or less and with Mathematica for concentrations >0.63. Error bars represent the standard error for at least eight distinct images. For samples at very high **F8H11** mole fraction (≥0.95), where features were close-packed, we determined the lateral sizes by measuring the peak-to-peak distance from image cross sections. For lower concentrations, where features were isolated, we determined the lateral size of the features by measuring the width of a feature before the height profile returned to the baseline of many individual features from AFM image cross sections. We made independent measurements of average cluster area by dividing the total areal coverage of clusters by the number of clusters. We further analyzed AFM images that exhibited periodic structures by performing Fourier transforms (FTs) using Image SXM software. For all samples except pure **F8H11**, angular

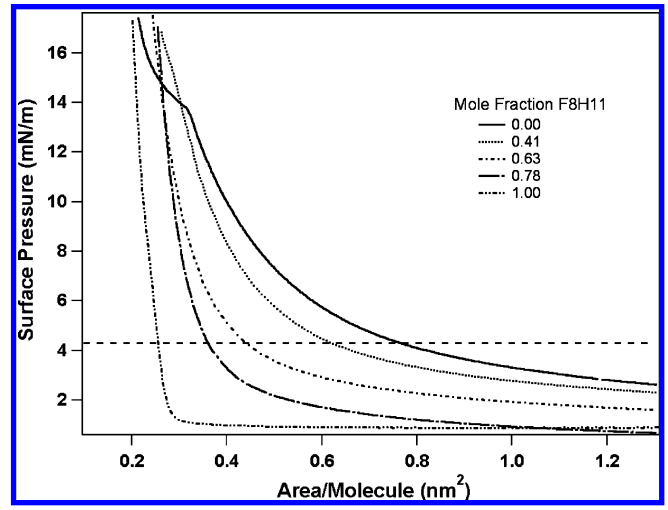

Figure 2. Representative isotherms of mixed **F8H11/F10** monolayers. The dashed line represents the surface pressure at which LB films were transferred.

averages were performed of these "powder pattern" FTs, and a linear background was subtracted. For pure **F8H11** monolayers, where distinct spots were observed, line averages were used rather than radial averages. The peak position, Q_0, and width (taken as 2σ, where σ is the standard deviation) was determined by a Gaussian fit from the resulting peaks; the row spacing was calculated as $2\pi/Q_0$, and the correlation length was calculated as $1/\sigma$.

Results

Figure 2 shows surface pressure versus molecular area isotherms of monolayers composed of **F10**, **F8H11**, and representative two-component mixtures. Isotherms of pure **F10** exhibited a gradual increase in surface pressure with decreasing molecular area that was suggestive of a 2D condensed phase (e.g., a 2D liquid or L_1 phase[40,41]) over a large range of molecular area. For **F8H11**, the surface pressure remained very low as the monolayer was compressed until it finally rose steeply at ∼0.3 nm^2/mol, which represents approximate molecular close-packing. This type of isotherm often indicates that the monolayer has condensed into domains of a dense 2D "solid" phase, initially separated by regions of 2D vapor.[42−44] The rise in surface pressure corresponds to the area at which these domains come into contact. Isotherms of mixtures where the mole fraction of **F8H11** was <0.63 exhibited features qualitatively similar to the pure **F10** isotherm, suggesting liquid-like behavior, whereas isotherms of mixtures with larger **F8H11** mole fractions exhibited solid-like behavior.

Whereas AFM images of pure **F10** LB monolayers were featureless, for **F8H11** mole fractions ≥0.02, AFM images exhibited compact features that were raised 1.4 ± 0.3 nm above the background. (See Figure 3.) The characteristic lateral dimension of the features, based on cross sections of AFM of individual features, was 34 ± 7 nm. The average feature area was 620 ± 90 nm^2. The latter value is a more reliable measure of feature size because it derives from an average over larger numbers of objects. The features were essentially monodisperse in size, within experimental error, in that both the apparent height and lateral dimension were approximately independent of **F8H11** concentration. However, the number density of features increased systematically with increasing **F8H11** mole fraction, as shown in Figure 4, suggesting that the features represent clusters of **F8H11** molecules. In particular, for mole

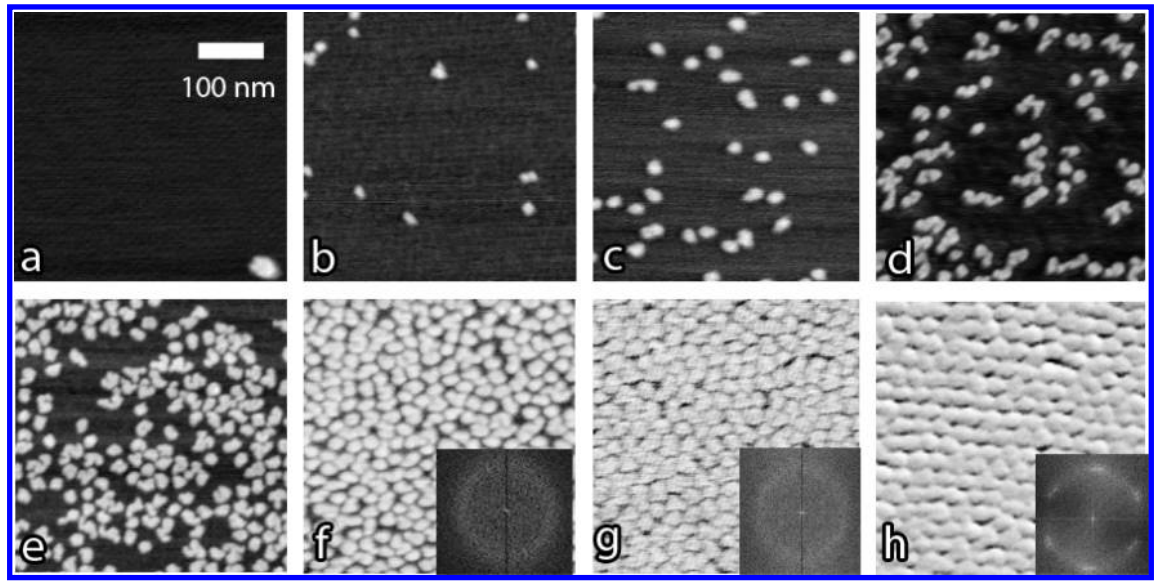

Figure 3. Representative AFM images of mixed **F8H11/F10** LB monolayers at **F8H11** mole fractions of (a) 0.02, (b) 0.15, (c) 0.26, (d) 0.41, (e) 0.63, (f) 0.78, (g) 0.95, and (h) 1.0. FTs are inset for the last three mole fractions.

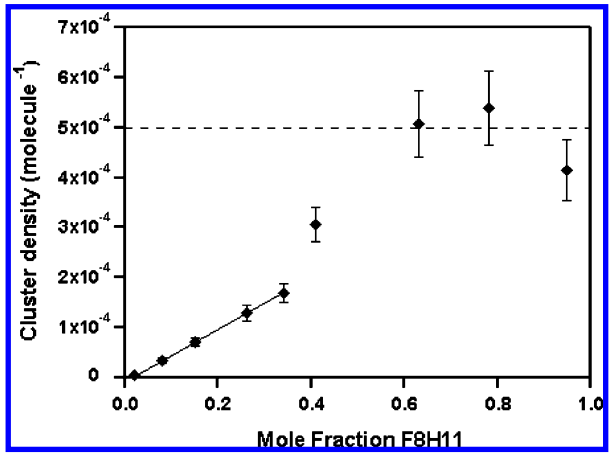

Figure 4. Number density of features per molecule in the film as a function of **F8H11** mole fraction. The solid line is a linear fit to the first five data points, and the dashed line represents the approximate close-packed cluster density.

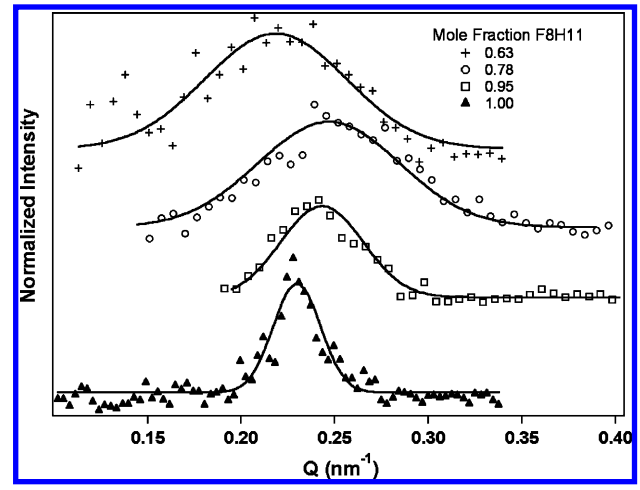

Figure 5. Radial Fourier transforms of representative AFM images of **F8H11/F10** mixtures that exhibit hexagonal order of clusters. The annotation indicates the **F8H11** mole fraction, and the lines indicate the best fit to a Gaussian function. Data for different concentrations are offset vertically for clarity and to facilitate comparison.

fractions of **F8H11** < 0.4, the number density of clusters increased linearly with linactant concentration. A linear fit to these data is consistent with a CMC of 0.013 ± 0.001 mole fraction **F8H11**, and the slope is consistent with an aggregation number of 2000 ± 100 **F8H11** molecules per cluster. At higher mole fractions, the number density of clusters appears to deviate from linearity. However, at these higher densities, clusters were often observed in close proximity to each other, complicating the process of feature counting and resulting in larger uncertainties.

At low **F8H11** mole fractions, the features were dilute and randomly located, with no evidence of long-range order. However, at high **F8H11** mole fractions, the features were locally organized in a hexagonal arrangement (indicated by the rings in the FTs included as insets in Figure 3); it is interesting to note that the onset of the local hexagonal order corresponds approximately to the **F8H11** concentration at which the surface pressure versus area isotherm exhibited solid-like behavior. Figure 5 shows representative radial FTs prepared as described above. Whereas the average position of the peak associated with the cluster packing changed little with **F8H11** concentration, the peak systematically narrowed with increasing concentration, indicating that the degree of organization increased with **F8H11** concentration. Table 1 gives the cluster spacing and the correlation length of local hexagonal order obtained from analyzing the FTs.

TABLE 1: Cluster Spacing and Correlation Length from Analysis of the FTs

mole fraction **F8H11**	Q_0 (nm^{-1})	row spacing (nm)	peak width (nm^{-1})	correlation length (nm)
0.63	0.22 ± 0.01	28 ± 1	0.049 ± 0.02	41 ± 16
0.78	0.23 ± 0.01	27 ± 1	0.055 ± 0.008	36 ± 5
0.95	0.24 ± 0.01	26 ± 1	0.033 ± 0.007	61 ± 13
1.0	0.235 ± 0.005	26.7 ± 0.5	0.017 ± 0.004	118 ± 28

Discussion

We hypothesize that the features observed in the AFM images represent self-limiting clusters composed predominantly of **F8H11**. (Figure 6 shows a schematic diagram of such a cluster.) Several observations support this hypothesis. The apparent height of the feature in the AFM images is consistent with the

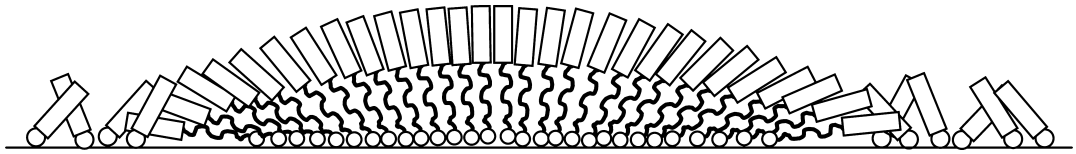

Figure 6. Proposed molecular configuration of a cluster.

difference in molecular length between **F8H11** and **F10**. Also, the number of features increases systematically with **F8H11** concentration. Furthermore, the lateral size of the features is monodisperse and invariant with **F8H11** concentration; we also verified that the feature size was unaffected by annealing time or compression speed. These observations suggest that the clusters represent equilibrium objects. Recent molecular dynamics simulations of partially fluorinated chains suggest that self-limiting aggregates such as the one pictured in Figure 6 might represent a stable configuration.[45]

Given the hypothesis that the clusters represent **F8H11** micelles, our data permit two independent calculations of the aggregation number: one from the dependence of cluster density on **F8H11** concentration and the other from direct measurements of cluster area divided by the molecular area. The comparison of values calculated in these ways represents an important test of the micelle hypothesis. The increase in the number of clusters with **F8H11** concentration, taken from the slope of the fit in Figure 4, is consistent with an aggregation number of 2000 ± 100 **F8H11** molecules per cluster. Using the average cluster area of 620 ± 90 nm^2 from the AFM measurements and an area per molecule of 0.28 nm^2 (taken from the isotherms) gives an aggregation number of 2200 ± 300. These two independent calculations of the aggregation number are nominally equivalent within experimental uncertainty. The consistency of these two values supports the hypothesis that the clusters represent micelles composed of **F8H11**.

A hypothetical 2D micelle of the type shown in Figure 6 is presumably due to an intrinsic packing frustration between hydrocarbon and fluorocarbon segments leading to spontaneous curvature. Although the terminology is similar, these 2D micelles are fundamentally different from the surface hemimicelles[46−59] (or admicelles) observed in one-component adsorbed layers, which are directly related to 3D micelles in the same systems and exhibit characteristic dimensions related to twice the molecular length. The characteristic lateral dimension of the clusters observed here is roughly an order of magnitude larger and contains ∼2000 molecules, whereas a typical 3D micelle has an aggregation number of 50−100. The 2D geometry permits greater flexibility in micelle size because the presence of the third embedding dimension provides additional options for structures that separate chemically incompatible moieties.

The hexagonal micelle packing observed at high concentration was consistent with a liquid crystalline (e.g., hexatic) phase of clusters. In a monolayer of 100% **F8H11**, the correlations were sufficiently long-range that orientational order was explicitly demonstrated by the presence of distinct spots in the FTs. These observations suggest that the increasing area fraction of clusters leads to a 2D phase transition from an isotropic micellar phase to a liquid crystalline phase. Supporting this model is the fact that the isotherms exhibit characteristically different shapes at low and high concentrations.

Conclusions

Two-component LMs composed of semifluorinated and perfluorinated amphiphiles exhibited behavior that was quantitatively consistent with the formation of 2D micelles. The semifluorinated compound, previously shown to be line-active at the interface between hydrocarbon and fluorocarbon domains within monolayers,[25,26] played the role of 2D surfactant (linactant), and the perfluorinated compound acted as the 2D analog of solvent. Above a critical linactant mole fraction of 0.013, AFM images showed the presence of monodisperse 2D molecular clusters within these monolayers. By analogy to 3D micelles, the number of clusters increased with linactant concentration, whereas their size remained the same. An aggregation number of ∼2000 **F8H11** molecules was calculated self-consistently from the trend of cluster number versus concentration and from the cluster size and molecular area. A transition from an isotropic 2D micellar phase to a phase where the clusters exhibited local hexagonal packing was observed at a linactant mole fraction of ∼0.63; the correlation length of the hexagonal packing increased with linactant mole fraction. In contrast to 3D micelles, the characteristic lateral dimension of the 2D micelles was significantly larger than the molecular dimensions, suggesting that the finite size of the aggregate arose from a packing incompatibility between the hydrocarbon and fluorocarbon blocks in the linactant tailgroup.

Acknowledgment. This research was supported by NSF awards DMR-0906735 (D.K.S.) and DMR-0906727 (T.R.L.) and by the Liquid Crystal Materials Research Center (NSF MRSEC, DMR-0455490). S.M.M. also acknowledges support from a Department of Education GAANN fellowship.

References and Notes

(1) Corrin, M. L.; Klevens, H. B.; Harkins, W. D. *J. Chem. Phys.* **1946**, *14*, 480–486.
(2) Israelachvili, J. N.; Mitchell, D. J.; Ninham, B. W. *J. Chem. Soc., Faraday Trans. 2* **1976**, *72*, 1525–1568.
(3) Luzzati, V.; Husson, F. *J. Cell Biol.* **1962**, *12*, 207–219.
(4) Debye, P. *Ann. N. Y. Acad. Sci.* **1949**, *51*, 575–592.
(5) Tanford, C. *J. Phys. Chem.* **1974**, *78*, 2469–2479.
(6) Tanford, C. *Proc. Natl. Acad. Sci. U.S.A.* **1974**, *71*, 1811–1815.
(7) Israelachvili, J. *Langmuir* **1994**, *10*, 3774–3781.
(8) Benvegnu, D. J.; McConnell, H. M. *J. Phys. Chem.* **1992**, *96*, 6820–6824.
(9) Brewster, R.; Pincus, P. A.; Safran, S. A. *Biophys. J.* **2009**, *97*, 1087–1094.
(10) Blanchette, C. D.; Lin, W. C.; Orme, C. A.; Ratto, T. V.; Longo, M. L. *Biophys. J.* **2008**, *94*, 2691–2697.
(11) Esposito, C.; Tian, A.; Melamed, S.; Johnson, C.; Tee, S. Y.; Baumgart, T. *Biophys. J.* **2007**, *93*, 3169–3181.
(12) Honerkamp-Smith, A. R.; Cicuta, P.; Collins, M. D.; Veatch, S. L.; den Nijs, M.; Schick, M.; Keller, S. L. *Biophys. J.* **2008**, *95*, 236–246.
(13) Idema, T.; van Leeuwen, J. M. J.; Storm, C. *Phys. Rev. E* **2009**, *80*, 041924.
(14) Tian, A. W.; Johnson, C.; Wang, W.; Baumgart, T. *Phys. Rev. Lett.* **2007**, *98*, 208102.
(15) Ursell, T. S.; Klug, W. S.; Phillips, R. *Proc. Natl. Acad. Sci. U.S.A.* **2009**, *106*, 13301–13306.
(16) Rinia, H. A.; de Kruijff, B. *FEBS Lett.* **2001**, *504*, 194–199.
(17) Ding, J. Q.; Doudevski, I.; Warriner, H. E.; Alig, T.; Zasadzinski, J. A. *Langmuir* **2003**, *19*, 1539–1550.
(18) Discher, B. M.; Maloney, K. M.; Grainger, D. W.; Hall, S. B. *Biophys. Chem.* **2002**, *101*, 333–345.
(19) Gopal, A.; Lee, K. Y. C. *J. Phys. Chem. B* **2001**, *105*, 10348–10354.

(20) Aoki, P. H. B.; Volpati, D.; Riul, A.; Caetano, W.; Constantino, C. J. L. *Langmuir* **2009**, *25*, 2331–2338.
(21) Caseli, L.; Perinotto, A. C.; Viitala, T.; Zucolotto, V.; Oliveira, O. N. *Langmuir* **2009**, *25*, 3057–3061.
(22) Blodgett, K. B. *J. Am. Chem. Soc.* **1935**, *57*, 1007–1022.
(23) Schwartz, D. K. *Surf. Sci. Rep.* **1997**, *27*, 245–334.
(24) Zasadzinski, J. A.; Viswanathan, R.; Madsen, L.; Garnaes, J.; Schwartz, D. K. *Science* **1994**, *263*, 1726–1733.
(25) Trabelsi, S.; Zhang, S.; Lee, T. R.; Schwartz, D. K. *Phys. Rev. Lett.* **2008**, *100*, 037802.
(26) Trabelsi, S.; Zhang, Z.; Zhang, S.; Lee, T. R.; Schwartz, D. K. *Langmuir* **2009**, *25*, 8056–8061.
(27) Trabelsi, S.; Zhang, S.; Lee, T. R.; Schwartz, D. K. *Soft Matter* **2007**, *3*, 1518–1524.
(28) Trabelsi, S.; Zhang, S. S.; Zhang, Z. C.; Lee, T. R.; Schwartz, D. K. *Soft Matter* **2009**, *5*, 750–758.
(29) Maaloum, M.; Muller, P.; Krafft, M. P. *Angew. Chem., Int. Ed.* **2002**, *41*, 4331–4334.
(30) Maaloum, M.; Muller, P.; Krafft, M. P. *Langmuir* **2004**, *20*, 2261–2264.
(31) Zhang, G. F.; Maaloum, M.; Muller, P.; Benoit, N.; Krafft, M. P. *Phys. Chem. Chem. Phys.* **2004**, *6*, 1566–1569.
(32) Fontaine, P.; Goldmann, M.; Muller, P.; Faure, M. C.; Konovalov, O.; Krafft, M. P. *J. Am. Chem. Soc.* **2005**, *127*, 512–513.
(33) Zhang, G. F.; Marie, P.; Maalourn, M.; Muller, P.; Benoit, N.; Krafft, M. P. *J. Am. Chem. Soc.* **2005**, *127*, 10412–10419.
(34) Semenov, A. N.; Gonzalez-Perez, A.; Krafft, M. P.; Legrand, J. F. *Langmuir* **2006**, *22*, 8703–8717.
(35) Krafft, M. P.; Riess, J. G. *Chem. Rev.* **2009**, *109*, 1714–1792.
(36) Gallyamov, M. O.; Mourran, A.; Tartsch, B.; Vinokur, R. A.; Nikitin, L. N.; Khokhlov, A. R.; Schaumburg, K.; Moller, M. *Phys. Chem. Chem. Phys.* **2006**, *8*, 2642–2649.
(37) Kato, T.; Kameyama, M.; Ehara, M.; Iimura, K. *Langmuir* **1998**, *14*, 1786–1798.
(38) Yoshimura, T.; Ohno, A.; Esumi, K. *Langmuir* **2006**, *22*, 4643–4648.
(39) Mourran, A.; Tartsch, B.; Gallyamov, M.; Magonov, S.; Lambreva, D.; Ostrovskii, B. I.; Dolbnya, I. P.; de Jeu, W. H.; Moeller, M. *Langmuir* **2005**, *21*, 2308–2316.
(40) Pallas, N. R.; Pethica, B. A. *Langmuir* **1985**, *1*, 509–513.
(41) Hifeda, Y. F.; Rayfield, G. W. *Langmuir* **1992**, *8*, 197–200.
(42) Barton, S. W.; Goudot, A.; Bouloussa, O.; Rondelez, F.; Lin, B. H.; Novak, F.; Acero, A.; Rice, S. A. *J. Chem. Phys.* **1992**, *96*, 1343–1351.
(43) Riviere, S.; Henon, S.; Meunier, J.; Schwartz, D. K.; Tsao, M. W.; Knobler, C. M. *J. Chem. Phys.* **1994**, *101*, 10045–10051.
(44) Fainerman, V. B.; Vollhardt, D. *J. Phys. Chem. B* **2003**, *107*, 3098–3100.
(45) Pineiro, A.; Prieto, G.; Ruso, J. M.; Verdes, P. V.; Sarmiento, F. *J. Colloid Interface Sci.* **2009**, *329*, 351–356.
(46) Manne, S.; Cleveland, J. P.; Gaub, H. E.; Stucky, G. D.; Hansma, P. K. *Langmuir* **1994**, *10*, 4409–4413.
(47) Manne, S.; Gaub, H. E. *Science* **1995**, *270*, 1480–1482.
(48) Ducker, W. A.; Grant, L. M. *J. Phys. Chem.* **1996**, *100*, 11507–11511.
(49) Ducker, W. A.; Wanless, E. J. *Langmuir* **1996**, *12*, 5915–5920.
(50) Grant, L. M.; Ducker, W. A. *J. Phys. Chem. B* **1997**, *101*, 5337–5345.
(51) Manne, S.; Schaffer, T. E.; Huo, Q.; Hansma, P. K.; Morse, D. E.; Stucky, G. D.; Aksay, I. A. *Langmuir* **1997**, *13*, 6382–6387.
(52) Wanless, E. J.; Davey, T. W.; Ducker, W. A. *Langmuir* **1997**, *13*, 4223–4228.
(53) Wanless, E. J.; Ducker, W. A. *Langmuir* **1997**, *13*, 1463–1474.
(54) Fuerstenau, D. W.; Colic, M. *Colloids Surf., A* **1999**, *146*, 33–47.
(55) Patrick, H. N.; Warr, G. G.; Manne, S.; Aksay, I. A. *Langmuir* **1999**, *15*, 1685–1692.
(56) Wolgemuth, J. L.; Workman, R. K.; Manne, S. *Langmuir* **2000**, *16*, 3077–3081.
(57) Fuerstenau, D. W. *J. Colloid Interface Sci.* **2002**, *256*, 79–90.
(58) Nelson, M.; Cain, N.; Taylor, C. E.; Ocko, B. M.; Gin, D. L.; Hammond, S. R.; Schwartz, D. K. *Langmuir* **2005**, *21*, 9799–9802.
(59) Cain, N.; Van Bogaert, J.; Gin, D. L.; Hammond, S. R.; Schwartz, D. K. *Langmuir* **2007**, *23*, 482–487.

JP104375S